RESEARCH PAPER

Angularly resolved ellipsometric optical biosensing by means of Bloch surface waves

**Alberto Sinibaldi · Aleksei Anopchenko · Riccardo Rizzo ·
Norbert Danz · Peter Munzert · Paola Rivolo · Francesca Frascella ·
Serena Ricciardi · Francesco Michelotti**

Abstract In label-free biosensing, a continuous improvement of the limit of detection is necessary to resolve the small change of the surface refractive index produced by interacting biomolecules at a very small concentration. In the present work, optical sensors based on one-dimensional photonic crystals supporting Bloch surface waves are proposed and adopted for label-free optical biosensing. We describe the implementation of an angularly resolved ellipsometric optical sensing scheme based on Bloch surface waves sustained by tantala/silica multilayers. The angular operation is obtained using a focused beam at fixed wavelength and detection of the angular reflectance spectrum by means of an array detector. The results show that the experimental limit of detection for a particular photonic crystal design is 6.5×10^{-7} refractive index units (RIU)/Hz$^{1/2}$ and further decrease could be obtained. For the first time, we report on the practical application of this technique to a cancer biomarker protocol that aims at the detection of a specific glycoprotein (angiopoietin 2) involved in angiogenesis and inflammation processes.

A. Sinibaldi · A. Anopchenko · R. Rizzo · F. Michelotti (✉)
Department of Basic and Applied Science for Engineering, Sapienza University of Rome, Via A. Scarpa 16, 00161 Rome, Italy
e-mail: francesco.michelotti@uniroma1.it

R. Rizzo · N. Danz · P. Munzert
Fraunhofer Institute for Applied Optics and Engineering IOF,
A.-Einstein-Str. 7, 07745 Jena, Germany

P. Rivolo · F. Frascella · S. Ricciardi
Department of Applied Science and Technology, Politecnico di Torino, Corso Duca degli Abruzzi 24, 10129 Torino, Italy

Keywords Optical biosensing · Label-free biosensors · Photonic crystals · Bloch surface waves · Ellipsometry · Biophotonics

Introduction

The growing demand for non-invasive early detection of diseases pushes the scientific community to develop more and more refined technical solutions to identify and reveal the respective biomarkers at lower and lower concentrations [1]. The optical approach to label-free biosensing is among the most promising ones to meet these requirements. Surface plasmon polariton (SPP) resonance label-free optical biosensors, usually named surface plasmon resonance (SPR) biosensors, have been developed and optimized in a variety of configurations and are routinely used in biology laboratories [2–5]. Among other label-free optical approaches [6–8], optical biosensors based on electromagnetic modes (Bloch surface waves (BSWs)) excited at the surface of one-dimensional photonic crystals (1DPCs) [9] were proposed and demonstrated as a practical route to enhanced resolution and constitute an attractive alternative to SPP [10–14].

With respect to SPP sustained by thin metal layers, the confinement of BSW at the interface between a finite 1DPC and an external dielectric medium is guaranteed by Bragg reflection and total internal reflection on the two sides of the interface, respectively [9]. Similar to SPP, the excitation of a BSW at a given wavelength (λ_0) can be achieved using a prism coupler in the Kretschmann-Raether configuration [15] and is revealed by the appearance of a dip in the angular reflectance spectrum. The angular position of such a dip is very sensitive to perturbations of the refractive index at the

1DPC-external medium interface and can be used for biosensing purposes.

The main competitive advantages of using BSW for biosensing applications lie in the small absorption of the dielectric materials constituting the 1DPC and in the possibility to tailor the 1DPC geometry in order to operate at practically any wavelength. The small absorption makes the dips in the reflectance much narrower than those observed for SPP, leading to a potentially larger performance of the biosensors in terms of a properly defined figure of merit (FoM) and limit of detection (LoD) [16–18]. Besides, in the case in which BSWs are exploited for fluorescence-based biosensing, the 1DPC does not quench the emission of labels at the 1DPC surface [19, 20]. The possibility to fabricate 1DPC using either different dielectric materials or different geometries, in terms of layer thicknesses, made that BSW biosensors be developed in a wide range of wavelengths, from the blue region [21] to the near-infrared [12] and terahertz range [22]. Carefully designing the 1DPC geometry also allows to utilize either transverse electric (TE) or transverse magnetic (TM)-polarized BSW and, eventually, combinations of the two polarizations [23].

Recently, we proposed to exploit both the TE and TM reflectivities of a 1DPC sensor and their phase relation around the BSW resonance in a polarization control scheme [24]. Such approach was already reported for SPP in a spectroscopic detection scheme [25]. When comparing with a single polarization scheme (TE or TM), it permits to increase the FoM and decrease the LoD. In the following, we shall restrict our study to 1DPC sustaining TE-polarized BSW. We shall describe the operation of BSW sensors in either a single polarization (TE) or in a polarization control scheme, referring to such configurations with the terms *TE scheme* and *cross scheme*, respectively. One should, however, keep in mind that, for a different 1DPC design, the single polarization scheme could operate along the TM direction as well, with FoM and LoD depending on the specific design. Investigations on the comparison of the optimized sensing performances between the TE and TM cases are on the way.

In the present study, we report on the development of BSW biosensors operating in an angular interrogation scheme where the reflectance of a focused laser beam at λ_0 is monitored using an array detector. We first characterize the sensor performance with respect to all possible polarization configurations and experimentally determine the volume sensitivity and LoD for bulk refractive index changes. Methods for effective immobilization of a binding layer of protein G on the 1DPC sensing surface are discussed then. Finally, experimental results on a proof-of-principle cancer biomarker assay for the detection of a specific glycoprotein (angiopoietin 2) are presented.

Materials and methods
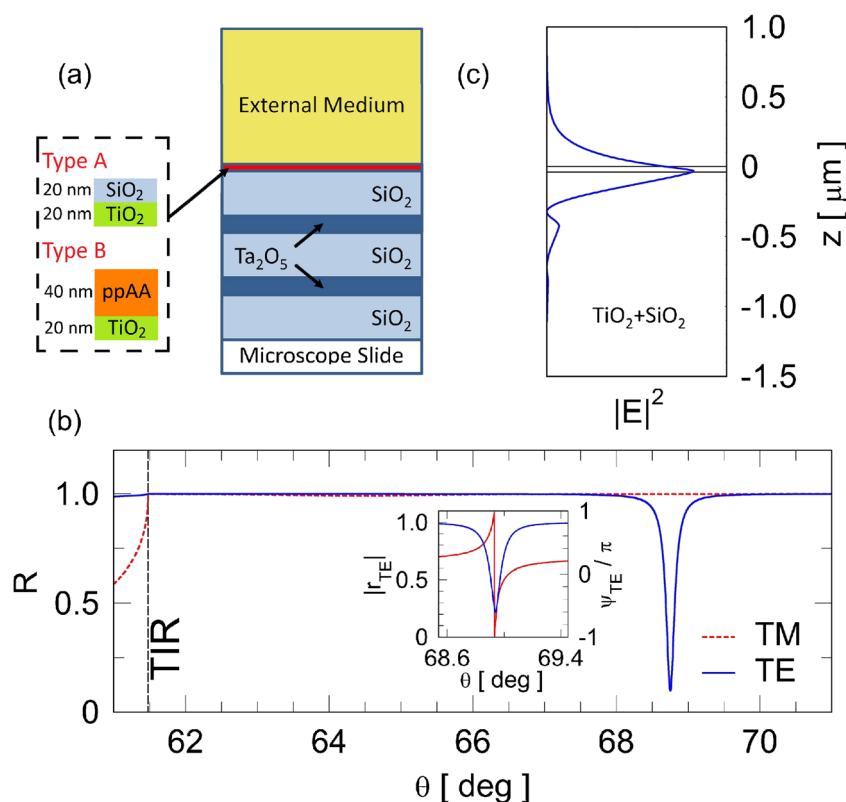
1DPC sensor design and fabrication

The 1DPC used in this study was fabricated by plasma ion-assisted evaporation under high vacuum conditions by means of an APS904 coating system (Leybold Optics) on standard microscope slides. The materials chosen for the fabrication were SiO_2 (silica), Ta_2O_5 (tantala) and TiO_2 (titania). To obtain dielectric layers with moderate stress and minor absorption losses, medium-level argon ion assistance with ion energies of about 120 eV was applied [26]. All dielectric coating materials were evaporated by electron beam gun evaporation with deposition rates of 0.5 nm/s for SiO_2, 0.4 nm/s for Ta_2O_5 and 0.25 nm/s for the TiO_2 layer. The single-layer thicknesses in the stack were terminated by quartz crystal monitoring. A preconditioning of the substrates was performed by plasma etching with the APS plasma source for 60 s and low ion energies.

The complex refractive indices were determined either by reflection/transmission spectroscopy on single layers or by ellipsometry on test multilayers sustaining BSW. We have $d_{Ta_2O_5} = 120$ nm and $n_{Ta_2O_5} = 2.160 + j5 \times 10^{-5}$; $n_{TiO_2} = 2.28 + j1.8 \times 10^{-3}$ at λ_0=670 nm.

The 1DPC was designed to show a sharp TE-polarized BSW dip at about θ=69° when operating at λ_0=670 nm, where θ is the incidence angle inside the prism coupler. In Fig. 1a, we show a sketch of the geometry of the 1DPC. Starting from the substrate side, the 1DPC is constituted by a first silica layer that is used to improve the reliability of the subsequent high index layer, a periodic part made out of two tantala/silica bilayers and a topping part made out of a thin titanium/silica bilayer. In the case reported here, the thicknesses used for the matching layer and the periodic part are $d_{SiO_2} = 275$ nm and $d_{Ta_2O_5} = 120$ nm. The thicknesses of the two topping layers are $d_{TiO_2} = 20$ nm and $d_{SiO_2} = 20$ nm. The thin titanium layer has been designed to obtain a narrow width and a large depth of the resonance, while the covering silica layer shall provide a suitable surface for well-established chemical functionalization methods, making use of the hydroxyl groups (e.g. APTES).

In Fig. 1b, we show the angular reflectance spectrum calculated at λ_0 in the Kretschmann-Raether configuration with a BK7 coupling prism. A sharp dip in the TE reflectance is clearly visible around θ=69°, corresponding to the excitation of a TE-polarized BSW, well above the total internal reflection (TIR) edge. A much shallower dip (less than 1 %) appears in the TM reflectance at about θ=64.5°, corresponding to a TM-polarized mode. In the inset of Fig. 1b, we plot both the amplitude and the phase of the complex TE field reflection coefficient; the phase clearly shows a 2π shift around the resonance that will be exploited in the polarization control scheme described below. In the same angular range, the amplitude and phase of the TM field reflection coefficient are almost

constant. All numerical calculations were performed by means of a custom code based on the transfer matrix method and using a plane-wave approach [24].

In Fig. 1c, we show the distribution of the TE-polarized BSW energy density calculated at λ_0 and in resonance conditions. The BSW is confined at the interface between the 1DPC and the external medium. The field is exponentially decaying in the external medium with a penetration length (L_{pen}) of 117 nm (a hypothetic SPP sensor operating at the same λ_0 and resonance angle would exhibit the same L_{pen}).

In the present work, we deposited and used two versions of the 1DPC sketched in Fig. 1a. In one case (type A), the 1DPC was fully fabricated and used for the physical characterization of their operation. In the second case (type B), the 1DPC was fabricated up to the titanium topping layer. The last silica topping layer was not deposited in order to accommodate a thin functional polymer layer used to provide the chemical groups needed to graft the biomolecules. In such a way, the polymer functional layer is embedded in the 1DPC geometry and the sensing characteristics are preserved (resonance angle, sensitivity, figure of merit).

Chemical functionalization and biological protocols

The thin functional polymeric layers were deposited using a plasma polymerization technique, making use of a radio-frequency plasma-enhanced chemical vapour deposition (RF-PECVD) reactor (chamber base pressure, P=26 mTorr;

radio frequency, f_{RF}=13.56 MHz) equipped with a delivery frame suitable to inject vapours coming from liquid reactants (monomer precursors). The reactor is a cylindrical closed chamber (320 mm wide and 200 mm high) made by stainless steel. Argon was selected as a gas carrier in order to sustain the plasma discharge that promotes the mechanism of radical chain polymerization. That results in the deposition of a thin layer of plasma-polymerized poly(acrylic acid) (plasma-pAA or ppAA) on the top of the 1DPC with different thicknesses depending on the working conditions.

The whole treatment consists of a two-step process (i) the surface etching by a continuous Ar plasma discharge (for promoting the adhesion of the ppAA coating on a sensor surface) and (ii) the acrylic acid monomer (99 %, by Sigma) polymerization by a pulsed plasma discharge.

Surface etching step was performed by Ar gas (flow= 20 standard cubic centimeters per minute (sccm)), applying a RF power of 50 W, for 5 min at a total pressure of 220 mTorr.

Polymerization was performed by diluting acrylic acid vapours (flow=3 sccm) in Ar flow (20 sccm) and by applying a discharge RF power of 200 W, a 10 % duty cycle (Time$_{on}$= 10 ms, Time$_{off}$=90 ms) for 4 min at a total pressure of 145 mTorr. The acrylic acid vapour partial pressure was 20 mTorr.

The ppAA-functionalized 1DPC was then soaked in Milli-Q grade deionized water (dH$_2$O) for 30 min under oscillating shaking in order to remove unstable surface oligomers formed at the end of the plasma process [27]. The ppAA coatings expose at the surface a large number of carboxylic groups (−

COOH) able to react with the amino groups (–NH$_2$) of biomolecules, through the formation of an amidic bond. The physical-chemical properties of ppAA films deposited on several substrates were previously characterized by means of ATR FT-IR spectroscopy, optical contact angle (OCA) analysis and XPS spectroscopy [27, 28]. The surface density of the carboxylic functionalities (~10^{16} cm^{-2}) was quantified by colorimetric titration with toluidine blue O (TBO) [27, 28].

The dependency of the ppAA layer thickness on the process parameters was calibrated by the AFM characterization of single films deposited on reference substrates. The thickness of the ppAA layers used was estimated by atomic force microscopy and is d_{ppAA}~40 nm. The refractive index of ppAA was obtained by spectroscopic ellipsometry and is n_{ppAA}=1.52.

Before ppAA deposition, the 1DPC surface was cleaned with a piranha solution of sulfuric acid H$_2$SO$_4$ and hydrogen peroxide H$_2$O$_2$ in a ratio of 3:1 for 5 min. Both chemicals were purchased from Sigma-Aldrich. The ppAA-coated 1DPC was chemically treated to activate the –COOH groups with a solution of sulfo-NHS (N-hydroxysulfosuccinimide) and EDC (1-ethyl-3-(3-dimethylaminopropyl)carbodiimide hydrochloride) in a BupH MES (2-(N-morpholino)ethanesulfonic acid) buffer at pH 4.7. The chemicals used in the functionalization were purchased from Thermo Scientific and were used as received. The product numbers are 24525, 22980 and 22980, respectively. The chemical treatment lasted for 15 min.

The protein G (PtG) used in our biosensing experiments was purchased from Thermo Scientific (product number 21193). PtG is a recombinant protein to probe mouse and human antibody, especially IgG isotype. The recombinant human angiopoietin 2 (Ang2), the target cancer biomarker, and its specific monoclonal anti-human antibody (Ig class mouse IgG$_{2B}$) anti-angiopoietin 2 (anti-Ang2), the probe antibody, were purchased from R&D (product numbers 623-AN and MAB0983, respectively). Dulbecco's phosphate-buffered saline (D-PBS) 1× (10 mM) was used as a solvent for the proteins and for washing and reference purposes. As a cleaning solution, a glycine 20 mM solution was used in double-deionized water (ddH$_2$O) with hydrogen chloride to reach a pH level of 2.5. The PBS buffer and glycine were purchased from Sigma-Aldrich (product numbers D1408 and 410225, respectively). The blocking agent adopted in the biosensing experiment is bovine serum albumin (BSA) from Sigma-Aldrich (product number A7906).

Experimental apparatus

The experimental results reported in the next section were obtained by making use of the experimental apparatus sketched in Fig. 2. The apparatus implements a polarization-resolved far-field total internal reflection ellipsometer.

The light beam emitted by a temperature-stabilized (±0.01 °C) laser diode (LD) at λ=670 nm (Thorlabs LPS-675-FC) is collimated and linearly polarized at 45° with respect to the incidence plane of the prism coupler by means of a first polarizer. A liquid crystal-phase retarder (LCR) (Newport 932-NIR) allows one to change the phase Ψ between the TE and TM components in order to access any state of elliptical polarization. The laser beam is then expanded by means of a telescope, and the central portion is selected by means of a circular aperture (diameter 1 cm). In the focal point of the telescope, a rotating diffuser is destroying the spatial coherence of the beam. The integration time of the array detector is set to temporally integrate the diffuser effect, thus ruling out the effect of speckles. We checked experimentally that the diffuser is not affecting the polarization of the probe beam.

The beam is then focused by means of a cylindrical lens (f_1=100 mm) onto the coupling prism in the Kretschmann-Raether configuration within an angular range ($\Delta\theta$) of ~3.8°. The θ–2θ rotation stages are used to set the average incidence angle around the resonance to be tracked. The 1DPC biochip back facet is contacted to the prism by means
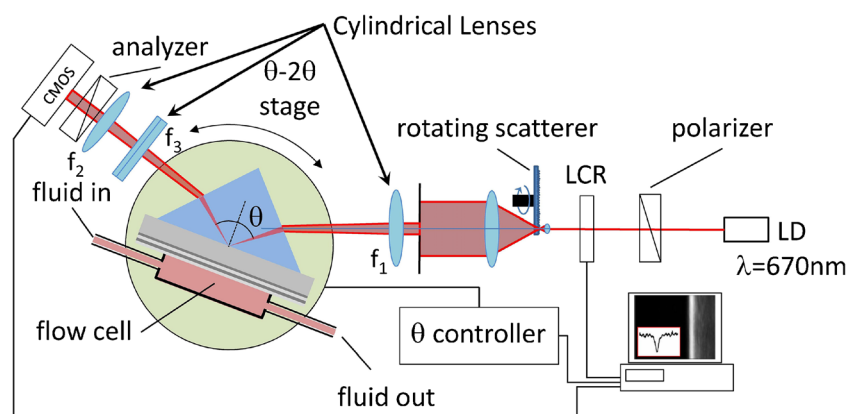

Fig. 2 Experimental apparatus, implementing the Kretschmann-Raether excitation scheme, used to characterize in the far field the performance of optical biosensors exploiting the BSW excitation. The orientation of the two cylindrical lenses with f_1 and f_2 is such that one-dimensional focusing is along the incidence plane. The cylindrical lens with f_3, used for imaging, is oriented in a way that focusing is perpendicular to the incidence plane

of a matching oil, and the biochip is topped by a temperature-controlled (± 0.01 °C) polydimethylsiloxane (PDMS) fluidic cell that permits to expose its surface to any analyte solution. The surface and volume of the cell are 0.48 cm^2 and 4.8 µL, respectively. The system is aligned in a way that the beam illuminates a sharp line at the biosensor surface perpendicularly to the incidence plane.

The reflected beam is collected using a second cylindrical lens ($f_2 = 150$ mm) and analyzed using a polarizer crossed with respect to the input one. Such cylindrical lens is performing Fourier imaging on the array detector; therefore, each pixel of the detector rows, lying in the incidence plane, corresponds to an angular component of the reflected beam. A third cylindrical lens ($f_3 = 70$ mm) images the sensor surface on the array detector; therefore, each pixel of the array columns corresponds to a position along the illuminated region. The array detector used here is an 8-bit CMOS array detector (Thorlabs DCC1645C). This optical configuration sets a width of the angular detection range of 1° along the largest dimension of the CMOS array (1280 pixels); therefore, 1 pixel corresponds to an angular width of 0.76 mdeg.

In Fig. 3, we show the images captured by the CMOS detector in the polarization-sensitive scheme (cross scheme) for the 1DPC described above (type A) and for several different values of the phase (Ψ): 0°, 90°, 180° and 270°. The angular intensity distribution can show either a dip (Fig. 3c), as found also in the single polarization (TE scheme) case, or a peak (Fig. 3a) and all the intermediate conditions, depending
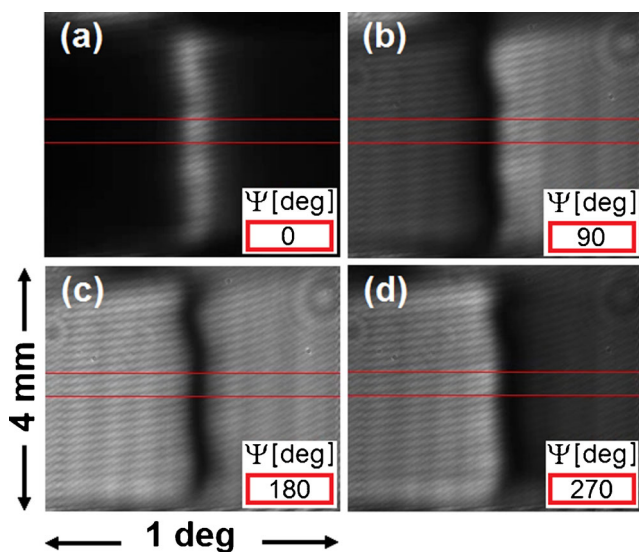
on the value of Ψ. Such dependency is due to the fact that the phase of the TE component is shifted by 2π when crossing the BSW resonance, whereas the phase of the TM component remains almost constant. A video (Electronic Supplementary Material (ESM) 1) shows the dependency of the images captured by the CMOS on the phase Ψ (with 1° step).

It is worth to note that in 1DPC with very small losses, the resonance observed in a TE scheme can be very shallow and hardly be tracked in a biosensing experiment [29]. Nevertheless, the same 1DPC, in the cross scheme, would show a large contrast of the angular reflectance and the resonance position can be efficiently tracked, leading to an improvement of the LoD. From the technological point of view, 1DPC with lowest possible losses is more simply deposited than tuning the stack losses accurately. Therefore, the cross scheme provides an efficient route to high contrast features without the need to control the losses.

Results and discussion

The following subsections shall report experimental results on the physical characterization of the BSW biosensors, in terms of sensitivity, noise and resolution, on the test of the chemical surface functionalization and, finally, on a real example of a cancer biomarker detection assay.

Physical characterization of the BSW biosensors

For the physical characterization of the BSW biosensors, we made use of 1DPC including the last silica topping layer (type A). In Fig. 4, we show the angular reflectance spectra at λ_0 for a 1DPC sensor (type A). The top parts of the figure refer to the TE case, whereas the bottom parts correspond to the cross scheme.

The theoretical reflectance spectra shown in Fig. 4a were numerically calculated by means of a custom algorithm based on the transfer matrix method applied to stratified dielectric media and working in the plane-wave approximation. In the calculations, we did not take into account the presence of reflection losses at the two glass-air interfaces of the coupling prism. With the values assumed for the complex refractive indices of the dielectric materials constituting the 1DPC, the theoretical TE reflectance shows a sharp and deep BSW resonance. Depending on the value of Ψ, the theoretical reflectance for the cross scheme shows either a dip or a peak and all intermediate shapes.

The experimental angular reflectance curves shown in Fig. 4b were obtained by operating the apparatus either in the TE or in the cross scheme. The curves were extracted from images of the CMOS array detector similar to those shown in Fig. 3, by averaging over 100 rows (the region between the two red lines shown in Fig. 3) for different values of Ψ.

The experimental curve for the TE polarization shows a resonance in the correct angular range and characterized by

Fig. 3 Images captured using the CMOS array detector, for the type A 1DPC, for four different values of the phase (Ψ) introduced by the liquid crystal retarder: (**a**) $\Psi = 0°$, (**b**) $\Psi = 90°$, (**c**) $\Psi = 180°$, (**d**) $\Psi = 270°$. The images were acquired by the CMOS at $\theta = 69°$, with an exposition time (t_{int}) of 80.1 ms, i.e. at a sampling frequency (f_{samp}) of 12.5 Hz. The tiny oblique interference fringes are due to multiple reflections in the output polarizer (not AR coated). The objective field of view is shown in (**c**) for convenience. A video (ESM 1) shows the dependency of the images captured by the CMOS on the phase (Ψ) (with 1° step)
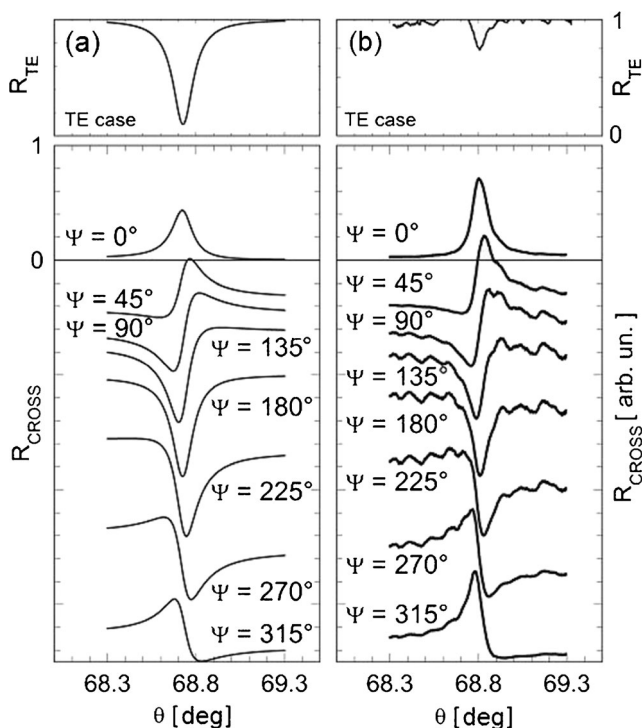
Fig. 4 (a) Calculated normalized reflectance spectra for the 1DPC (type A) described in the text for several different phases (Ψ) imposed by the liquid crystal retarder between the TE and TM components of the illumination beam. The Fresnel losses at the coupling prism facets are not taken into account. (b) Normalized experimental angular reflectance for the real 1DPC (type A) for different phases (Ψ). In both cases (a) and (b), the curves are shifted vertically for the sake of clarity

the expected full width at half maximum. However, the resonance is much shallower (about one fourth) than that found from the theory, indicating that the absorption introduced by the thin titanium topping layer is smaller than expected. Such result confirms the difficulty to tune the depth of the BSW resonance dip by controlling the 1DPC losses upon deposition.

The experimental curves for the cross case were compared very well to the theoretical curves too. In this case, the smaller absorption enhances the features around the BSW resonance with respect to the theoretical prediction. By varying the phase Ψ in the [0°, 360°] interval, we can experimentally access to all the reflectance distributions allowed by that 1DPC structure, as shown in the video that can be accessed by clicking on the caption of Fig. 3. Therefore, by making use of the same 1DPC sensor, one can select the appropriate phase conditions depending on the different experimental needs. For example, if one wishes to monitor a steep change in the reflectance profile, in amplitude mode at fixed λ_0 and θ_0 [3], he could set the phase around $\Psi=90°$ and monitor the changes of the reflected intensity [24].

In the following, we report experimental results obtained in the cross scheme by setting $\Psi=180°$ and measuring the angular shift of the minimum of the resonance dip as a function of the properties of the analytes injected in the PDMS fluidic cell.

The advantage of using the cross with respect to the TE scheme can be better evidenced by defining a FoM and comparing its value in the two cases. We adopt here the same FoM we previously used [24, 29], defined as $FoM = S_V \times D/W$, where S_V is the sensitivity of the BSW resonance angle to changes of the bulk refractive index of the external medium, D is the depth of the resonance dip (varying between 0 and 1), and W is the resonance full width at half maximum.

In Fig. 5a, we show the angular reflectance measured for the 1DPC sensor (type A) in both the cross and TE schemes. From the Lorentzian fit of the experimental curves, we find that $D_{TE}=0.28$, $W_{TE}=0.07°$, $D_{cross}=0.81$, and $W_{cross}=0.088°$. We find that W does not change much in the two cases, while D has a strong improvement in the cross case. We expect therefore that the cross resonance can be tracked more accurately (less noise).

The sensitivity (S_V) of the 1DPC sensor (type A) was determined, in both detection schemes, by injecting in the fluidic cell solutions of glucose in ddH$_2$O at several different known concentrations (0.05, 0.5 and 5 wt%). In Fig. 5b, we show the time dependence of the resonance position measured in the cross scheme, when either ddH$_2$O or the glucose solutions are injected in the fluidic cell. From the measurement, we derived the linear dependency of the resonance angle on the refractive index of the solutions as previously done in a precedent work [12]. From the slope of the linear behavior, we find the same volume sensitivity for the two detection schemes, as expected
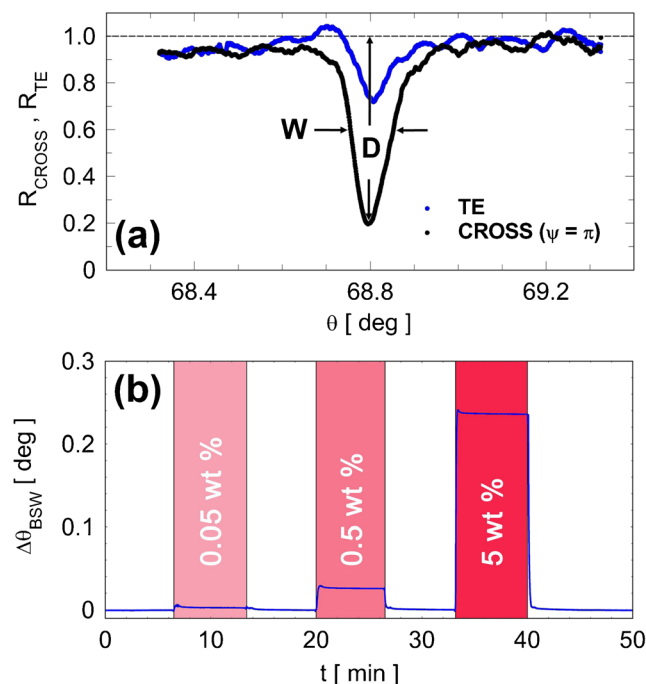

Fig. 5 (a) Experimental reflectance spectra in both TE (*blue curve*) and cross (*black curve*) schemes. D is the resonance depth, and W is the full width at half maximum. (b) Evaluation of the volume sensitivity obtained by injecting in the fluidic cell three different concentrations of glucose in ddH$_2$O (*on the right side*)

also from our numerical calculations, S_V=31.8°/remote interface units (RIU).

From the values measured for S_V, D and W, we can evaluate the FoM for the two schemes. We find FoM$_{TE}$=126 RIU^{-1} and FoM$_{cross}$=293 RIU^{-1}, indicating that the cross scheme outperforms the TE by more than a factor of 2. Considering that the LoD is inversely proportional to the FoM [30], we expect the LoD to be improved.

We determined the LoD in the cross scheme by measuring the noise of the measurement of the angular position of the resonance in static conditions and at fixed temperature (±0.01 °C). We find $\sigma(\theta_{BSW})$=7.31°×10^{-5}°, when fitting the resonance in a ±0.015° range (±20 pixels) around the minimum with a quadratic model and running the CMOS detector at a sampling frequency (f_{samp}) of 12.5 Hz. Such value corresponds to a 1 Hz equivalent bandwidth noise with $\sigma_{1\ Hz}(\theta_{BSW})$=2.07°×10^{-5}°/Hz$^{1/2}$. We can therefore say that the LoD=$\sigma_{1\ Hz}(\theta_{BSW})/S_V$=6.5× 10^{-7} RIU/Hz$^{1/2}$. Such value is smaller than that found experimentally for the TE case, LoD$_{TE}$=2.6×10^{-6} RIU/Hz$^{1/2}$, and can be further improved by optimizing the 1DPC sensor structure [30] and by detection of features (array detector with lower noise (CCD) and larger number of pixels, larger fitting interval, better fitting algorithms).

Test of the surface chemical functionalization

For such tests, we made use of 1DPC sensors without the last silica topping layer and coated with a 40-nm-thick ppAA functional layer (type B). The tests aim to verify that PtG is covalently bound at the biosensor surface by means of the ppAA carboxylic groups. The role of PtG is to subsequently bind probe antibodies and to orient them so as to expose in the right way their epitopes in a biological environment.

The tests were performed operating in the cross scheme with Ψ=180°, giving rise to a sharp dip in the reflectance spectrum. Again, the angular intensity distribution is obtained by averaging 100 rows of the CMOS array.

The tests are carried out according to the following protocol. Immediately before mounting the 1DPC sensor on the optical apparatus, stabilization and activation of the polymeric surface with EDC and sulfo-NHS in MES buffer was performed. Starting from the chemically functionalized 1DPC sensor, PtG dissolved in D-PBS 1× is injected in the fluidic cell and binds to the COOH groups of the ppAA layer.

In Fig. 6, we show the sensogram of a typical experiment. During all the tests, a slight positive drift of the resonance position was observed, due to buffer penetration inside the voids of the 1DPC layers (from top of the 1DPC), giving rise to an increase of their refractive index. Such drift was already reported by the authors [24, 29] and was removed by normalizing the experimental data. At the beginning, the fluidic cell is filled with D-PBS 1× and the angular position of the BSW resonance is taken as a reference.
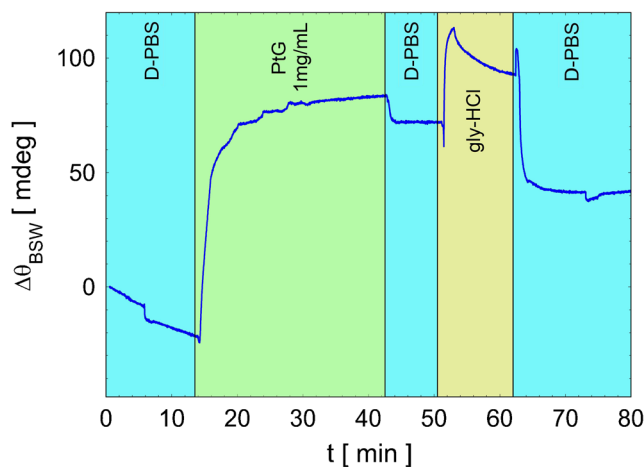

Fig. 6 Time dependence of the BSW resonance angular position in the cross reflectance obtained for Ψ=180° in a PtG binding test with a type B 1DPC sensor. $\Delta\theta_{BSW}$ is the relative angular shift of the BSW resonance

Upon injection of PtG dissolved in D-PBS 1× buffer (C= 1 mg/mL), we observe the kinetics of the binding reaction between the –COOH groups of the ppAA layer and the NH$_2$ groups of PtG. A positive shift of the BSW resonance takes place, indicating the growth of a PtG layer at the surface. During PtG incubation, a recirculation procedure is carried out for 30 min, where 35 µL of the PtG solution is pumped back and forth in the fluidic path. The volume of the fluidic cell is 8 µL. At the end of the PtG incubation, the fluidic cell is washed with D-PBS 1× and then filled with the glycine/HCl solution with the aim to remove the unspecifically bound PtG adlayers. Then, the cell is washed again with D-PBS 1×.

After the PtG incubation and the cleaning procedure, we observe the residual shift ($\Delta\theta$) of the resonance reported in Table 1, confirming that a PtG layer is formed at the biosensor surface. From $\Delta\theta$, we retrieved the mass surface coverage (Γ) for PtG by making use of the following formula [32] derived from de Feijter's formula [31]:

$$\Gamma = \frac{\Delta\theta \cdot L_{pen}}{S_v \cdot \partial n / \partial C} \qquad (1)$$

where $\partial n/\partial C$ is the refractive index increment of the molecules and $\partial n/\partial C$=0.19 cm^3/g for most of the proteins [31]. From Γ, we calculate the surface density Σ=Γ/MW, where MW is the molecular weight. From $\Delta\theta$, one can also retrieve, by assuming for PtG the refractive index (n_{BIO}=1.42), the adsorbed layer thickness (h). In Table 1, we report the values retrieved for Γ, Σ and h.

Cancer biomarker detection assay

As a proof-of-principle of the operation of the 1DPC sensors for biosensing applications, in the following, we discuss one exemplary assay carried out with one selected biomarker, the

Table 1 Summary of the protein properties and results extracted from the sensogram shown in Fig. 6

Protein	MW (kDa)	C^a (μg/mL)	C_M^b (μM)	$\Delta\theta^c$ (mdeg)	Γ^d (ng/cm^2)	Σ^e (10^{12}/cm^2)	h^f (nm)
G	21.6	1000	46.3	62	120	3.4	2.5
Anti-Ang2	150	2	0.013	7.1	13.7	0.055	0.29
Ang2	50	1	0.020	5.4	10.5	0.126	0.22

MW the molecular weight

[a] The mass of the solutions in D-PBS 1×

[b] The molar concentrations of the solutions in D-PBS 1×

[c] The residual angular shift of the BSW resonance after PBS and glycine-HCl washing

[d] The mass surface coverage

[e] The surface density

[f] The adsorbed layer thickness calculated assuming as a refractive index for all the biological layers (PtG, anti-Ang2, Ang2); n_{BIO}=1.42 [31]

recombinant human protein angiopoietin 2, which is indicative of angiogenesis associated to human cancer progression [33].

In this case, the 1DPC sensor (type B) surface is chemically activated with EDC/sulfo-NHS as described above and, differently from the case described in the previous section, the PtG immobilization is carried out externally, before mounting it on the optical setup. This permits to perform PtG immobilization only on some selected regions of the 1DPC sensor surface. For the assay described here, the 1DPC sensor surface which is accessed by the optical measurement was divided in two regions, in order to define one signal and one reference spots. In the two regions, we incubated simultaneously PtG (signal spot) and BSA (reference spot) in a moisturized atmosphere for 1 h at ambient temperature. The concentrations of the solutions used for immobilization of either PtG or BSA were 0.5 and 10 mg/mL, respectively. The concentration of the PtG solution was determined according to the experience gained in the measurements reported in the previous section. After incubation, the 1DPC sensors were washed thoroughly with D-PBS 1× and the incubation of BSA was repeated under the same conditions all over the 1DPC sensor surface in order to saturate all the ppAA functional groups. At the end, the resulting biochips were washed again thoroughly with D-PBS 1×.

After preparation, the biochip was topped with a one-channel microfluidic cell which permits to flow the analytes on top of the signal and reference spots, as sketched in Fig. 7a. The biochip was then mounted in the optical setup and operated in the cross scheme at Ψ=180°. The contact surface and volume of the fluidic channel are 18.7 mm^2 and 12 μL, respectively. In Fig. 7b, we show the CMOS camera image obtained when operating the biochip in D-PBS 1×. In the two regions where PtG and BSA were immobilized, a BSW resonance dip is observed; the resonance is missing in the intermediate region where the hydrophobic mark used to define the two regions is situated. In all the tests, a given volume (V, μL) of the analyte solution was injected in the channel at a

flow rate (F, μL/s) from the reference spot side by means of a motorized syringe pump.

In Fig. 7c, we show an exemplary assay performed with a biochip prepared as described above. Before starting the assay,
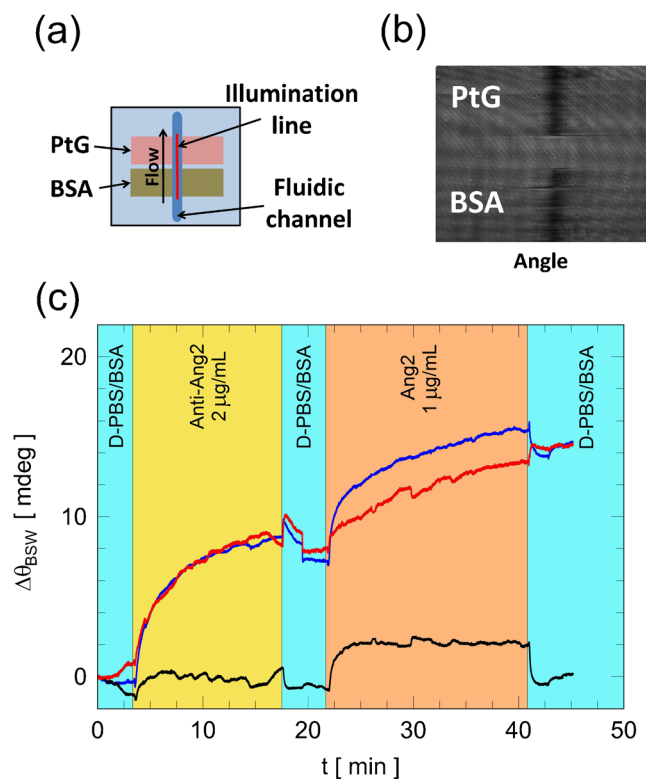

Fig. 7 (a) Sketch of the alignment of the fluidic channel, the sharp illumination line and the two spots used for signal and reference measurements for the biochips used in the cancer biomarker detection assays. (b) CMOS camera image obtained when the reference and signal spots are illuminated simultaneously. The image was obtained in D-PBS 1× environment before performing the assay. (c) Time dependence of the BSW resonance angular position in the cross reflectance obtained for Ψ=180° in a cancer biomarker assay with anti-Ang2 and Ang2. The *black curve* is the reference, the *blue curve* is the signal, and the *red curve* is the difference of the two. $\Delta\theta_{BSW}$ is the relative angular shift of the BSW resonance

the fluidic cell is filled with D-PBS 1×. Then, a 20 mM solution of glycine in water and HCl (pH 2.5) is injected in the cell to remove the proteins that are not covalently bound to the biochip surface. After 5 min, the solution is removed by injecting the buffer used during the assay, D-PBS 1× with 0.1 wt% BSA, and the assay is started ($t=0$). The angular position of the BSW resonance in the signal (blue) and reference (black) spots is tracked as a function of time upon injection of the analytes. The difference between the reference and the signal is also plotted (red) in Fig. 7c.

At $t=3.3$ min, a solution of anti-Ang2 in the buffer, with a concentration of 2 μg/mL, was injected, and at $t=17.5$ min, it was removed by injecting the buffer again. At $t=21.7$ min, a solution of Ang2 in the buffer, with a concentration of 1 μg/ mL, was injected, and at $t=40.8$ min, it was removed by injecting the buffer again. The injections of the anti-Ang2 and Ang2 solutions were performed with $V=100$ μL and $F= 1.13$ μL/s. All over the incubation time, a recirculation procedure was applied by pumping back and forth 25 μL from the syringe pump at $F=0.5$ μL/s. The injections of the buffer were performed with $V=500$ μL and $F=2.95$ μL/s. While washing with the buffer, the signal and the reference were measured along a time interval larger than the injection time; therefore, the step in the signals is due to stopping the flow and the last part of the measurement in the buffer is in static conditions.

During the assay, the reference shows a slight response due to transient temperature/pressure effects and to the different refractive indices of the solutions. On the other hand, upon injection of both analytes, the signal shows an exponential growth, indicating that the binding of anti-Ang2 to PtG and of Ang2 to anti-Ang2 is taking place during incubation. Fluctuations observed in both spots are due to pressure effects induced by the recirculation procedure.

Clearly, the differential signal, due only to binding of anti-Ang2 to PtG and of Ang2 to anti-Ang2, shows residual shifts after buffer washing whose values are reported in Table 1. From such shifts, by making use of Eq. (1), we evaluated the Γ, Σ and h for the anti-Ang2 and Ang2 add layers, as reported in Table 1.

The results show that the BSW biochip, prepared as reported above, can efficiently detect Ang2 in a buffer solution at the 1 μg/mL concentration. We can infer information on the limit of Ang2 detection by considering the measurement noise. The standard deviation of the noise observed during the assay is $\sigma(\theta_{BSW})=1°\times10^{-4°}$ when operating the CMOS at $f_{samp}= 12.5$ Hz, calculated from the difference signal measured in the time interval $t\in[41, 45$ min$]$ at the end of the assay in static conditions. Such value is slightly larger than that reported above for the type A sensor, in which only physical components contribute to the noise. From Eq. (1), assuming that the minimum detectable resonance shift is $\sigma(\theta_{BSW})$, one can calculate the limit of the biochip for Ang2 detection as $\Gamma_{LoD}= 1.9$ pg/mm^2 at $f_{samp}=12.5$ Hz. Such Γ_{LoD} must be compared to

the present state of the art for label-free techniques that is around 1–2 pg/mm^2 [34, 35]. The Γ_{LoD} found here can be decreased by decreasing the detection noise and by improving the referencing configuration. As an example, if $\sigma(\theta_{BSW})$ would get to the value we found for the type A sensor, we would have $\Gamma_{LoD}=1.4$ pg/mm^2. Changing the CMOS integration time could lead to further improvement.

Conclusions

We reported the development of BSW biosensors operating with Bloch surface waves in a novel full ellipsometric and angular interrogation scheme at a fixed wavelength. The phase properties of Bloch surface waves are exploited to improve the contrast of the intensity resonances observed in the Kretschmann-Raether total internal reflection configuration with a prism coupler. From physical characterization measurements, we obtained for the complete 1DPC sensor a sensitivity to bulk changes of the refractive index of the external medium ($S_V=31.8°$/RIU) and a limit of detection (LoD) of $6.5°\times 10^{-7°}$ RIU/Hz$^{1/2}$. This is a factor 2 improvement when compared to the results obtained in a single polarization TE scheme with the same 1DPC sensor. Future steps will combine this promising detection technique with a parallel label-free biosensing approach [36] in order to achieve sensitive multi-parameter analyses.

In the biosensing experiments, the thin poly(acrylic acid) layers deposited by plasma polymerization used to chemically functionalize the 1DPC sensors have demonstrated to efficiently bind to protein G molecules. Proof-of-principle cancer biomarker recognition assays, carried out in a classic immunoprecipitation scheme, showed that the biochips can efficiently detect angiopoietin 2 in a buffer solution. Under the present assay conditions, the limit of detection of the biochip for angiopoietin 2 was shown to be as low as 1.9 pg/mm^2.

References

1. Giljohann DA, Mirkin CA (2009) Drivers of biodiagnostic development. Nature 462:461–464
2. Liedberg B, Nylander C, Lunström I (1983) Surface plasmon resonance for gas detection and biosensing. Sensors Actuators 4:299

3. Homola J, Yee SS, Gauglitz G (1999) Surface plasmon resonance sensors: review. Sensors Actuators B 54:3–15

4. Wolfbeis OS (2006) Springer series on chemical sensors and biosensors. In: Wolfbeis OS, Homola J (eds) Surface plasmon resonance based sensors. Springer, Berlin

5. Piliarik M, Homola J (2009) Surface plasmon resonance (SPR) sensors: approaching their limits? Opt Express 17:16505–16517

6. Kabashin AV, Evans P, Pastkovsky S, Hendren W, Wurtz GA, Atkinson R, Pollard R, Podolskiy VA, Zayats AV (2009) Plasmonic nanorod metamaterials for biosensing. Nat Mater 8:867–871

7. Vollmer F, Arnold S (2008) Whispering-gallery-mode biosensing: label-free detection down to single molecules. Nat Methods 5:591–596

8. Luchansky MS, Bailey RC (2012) High-Q optical sensors for chemical and biological analysis. Anal Chem 84:793–821

9. Yeh P, Yariv A, Hong CS (1977) Electromagnetic propagation in periodic stratified media. I. General theory. J Opt Soc Am 67(4):423–438

10. Shinn M, Robertson WM (2005) Surface plasmon-like sensor based on surface electromagnetic waves in a photonic band-gap material. Sensors Actuators B 105:360–364

11. Konopsky VN, Alieva EV (2007) Photonic crystal surface waves for optical biosensors. Anal Chem 79(12):4729–4735

12. Giorgis F, Descrovi E, Summonte C, Dominici L, Michelotti F (2010) Experimental determination of the sensitivity of Bloch surface wave based sensors. Opt Express 18(8):8087–8093

13. Guo Y, Ye JY, Divin C, Huang B, Thomas TP, Baker JR, Norris TB (2010) Real-time biomolecular binding detection using a sensitive photonic crystal biosensor. Anal Chem 82:5211–5218

14. Rivolo P, Michelotti F, Frascella F, Digregorio G, Mandracci P, Dominici L, Giorgis F, Descrovi E (2012) Real time secondary antibody detection by means of silicon-based multilayers sustaining Bloch surface waves. Sensors Actuators B 161:1046–1052

15. Raether H (1988) Surface plasmons. Springer, Berlin

16. Shalabney A, Abdulhalim I (2012) Figure-of-merit enhancement of surface plasmon resonance sensors in the spectral interrogation. Opt Lett 37:1175–1177

17. Ameling R, Langguth L, Hentschel M, Mesch M, Braun V, Giessen PH (2010) Cavity enhanced localized plasmon resonance sensing. Appl Phys Lett 97:253116–253121

18. Sinibaldi A, Danz N, Descrovi E, Munzert P, Schulz U, Sonntag F, Dominici L, Michelotti F (2012) Direct comparison of the performance of Bloch surface wave and surface plasmon polariton sensors. Sensors Actuators B 174:292–298

19. Ballarini M, Frascella F, Michelotti F, Digregorio G, Rivolo P, Paeder V, Musi V, Giorgis F, Descrovi E (2011) Bloch surface waves-controlled emission of organic dyes grafted on a one-dimensional photonic crystal. Appl Phys Lett 99:043302

20. Ballarini M, Frascella F, Enrico E, Mandracci P, De Leo N, Michelotti F, Giorgis F, Descrovi E (2012) Bloch surface waves-controlled fluorescence emission: coupling into nanometer-sized polymeric waveguides. Appl Phys Lett 100:063305

21. Farmer A, Friedli A, Wright SM, Robertson WM (2012) Biosensing using surface electromagnetic waves in photonic band gap multilayers. Sensors Actuators B 173:79–84

22. Paeder V, Darmo J, Unterrainer K (2013) Ultra-thin terahertz waveguides on periodic dielectric multilayers. IEEE 38th International Conference on Infrared, Millimeter, and Terahertz Waves (IRMMW-THz)

23. Sinibaldi A, Fieramosca A, Rizzo R, Anopchenko A, Danz N, Munzert P, Magistris C, Barolo C, Michelotti F (2014) Combining label-free and fluorescence operation of Bloch surface wave optical sensors. Opt Lett 39:2947–2950

24. Sinibaldi A, Rizzo R, Figliozzi G, Descrovi E, Danz N, Munzert P, Anopchenko A, Michelotti F (2013) Full ellipsometric approach to optical sensing with Bloch surface waves on photonic crystals. Opt Express 21:23331

25. Homola J, Yee SS (1998) Novel polarization control scheme for spectral surface plasmon resonance sensors. Sensors Actuators B 51:331–339

26. Munzert P, Schulz U, Kaiser N (2003) Transparent thermoplastic polymers in plasma assisted coating processes. Surf Coat Technol 174–175:1048–1052

27. Ricciardi S, Castagna R, Severino SM, Ferrante I, Frascella F, Celasco E, Mandracci P, Vallini I, Mantero G, Pirri CF, Rivolo P (2012) Surface functionalization by poly-acrylic acid plasma-polymerized films for microarray DNA diagnostics. Surf Coat Technol 207:389–399

28. Frascella F, Ricciardi S, Rivolo P, Moi V, Giorgis F, Descrovi E, Michelotti F, Munzert P, Danz N, Napione L, Alvaro M, Bussolino F (2013) A fluorescent one-dimensional photonic crystal for label-free biosensing based on Bloch surface waves. Sensors 13:2011–2022

29. Michelotti F, Sinibaldi A, Munzert P, Danz N, Descrovi E (2013) Probing losses of dielectric multilayers by means of Bloch surface waves. Opt Lett 38:616–618

30. Rizzo R, Danz N, Michelotti F, Maillart E, Anopchenko A, Waecther C (2014) Optimization of angularly resolved Bloch surface wave biosensors. Opt Express 22:23202–23214

31. Voros J (2004) The density and refractive index of absorbing protein layers. Biophys J 87:553–561

32. Maillart E (2004) Développement d'un biocapteur par imagerie SPR. PhD thesis speciality: Optics, Université Paris XI, France

33. Galimi F, Torti D, Sassi F, Isella C, Corà D, Gastaldi S, Ribero D, Muratore A, Massucco P, Siatis D, Paraluppi G, Gonella F, Maione F, Pisacane A, David E, Torchio B, Risio M, Salizzoni M, Capussotti L, Perera T, Medico E, Di Renzo MF, Comoglio PM, Trusolino L, Bertotti A (2011) Genetic and expression analysis of MET, MACC1, and HGF in metastatic colorectal cancer: response to met inhibition in patient xenografts and pathologic correlations. Clin Cancer Res 17:3146–3156

34. Homola J (2008) Surface plasmon resonance sensors for detection of chemical and biological species. Chem Rev 108:462–493

35. Luchansky MS, Washburn AL, Martin TA, Iqbal M, Gunn LC, Bailey RC (2010) Characterization of the evanescent field profile and bound mass sensitivity of a label-free silicon photonic microring resonator biosensing platform. Biosens Bioelectron 26:1283–1291

36. Danz N, Kick A, Sonntag F, Schmieder S, Höfer B, Klotzbach U, Mertig M (2011) Surface plasmon resonance platform technology for multi-parameter analyses on polymer chips. Eng Life Sci 11:566–572